Electronic Structure of the CdS/Cu(In,Ga)Se 2 Interface of KF- and RbF-Treated Samples by Kelvin Probe and Photoelectron Yield Spectroscopy

Marin Rusu, Tim Kodalle, Leo Choubrac, Nicolas Barreau, Christian A Kaufmann, Rutger Schlatmann, Thomas Unold

Electronic Structure of the CdS/Cu(In,Ga)Se_2-Interface of KF and RbF-Treated Samples by Kelvin Probe and Photoelectron Yield Spectroscopy

Marin Rusu,[1,*] Tim Kodalle,[2] Leo Choubrac,[1] Nicolas Barreau,[3] Christian A. Kaufmann,[2] Rutger Schlatmann,[2] Thomas Unold[1]

[1]*Struktur und Dynamik von Energiematerialien, Helmholtz-Zentrum Berlin für Materialien und Energie, Lise-Meitner Campus, Hahn-Meitner-Platz 1, 14109 Berlin, Germany*

[2]*PVcomB, Helmholtz-Zentrum Berlin für Materialien und Energie, Schwarzschildstr. 3, 12489 Berlin, Germany*

[3]*Université de Nantes, CNRS, Institut des Matériaux Jean Rouxel, IMN, F-44000 France*

KEYWORDS: *chalcopyrites, thin-film solar cells, alkali fluoride postdeposition treatments, interfaces, band diagram, Kelvin probe, photoemission spectroscopy*

ABSTRACT: Ambient pressure Kelvin probe and photoelectron yield spectroscopy methods were employed to investigate the impact of the KF and RbF post-deposition treatments (KF-PDT, RbF-PDT) on the electronic features of $Cu(In,Ga)Se_2$ (CIGSe) thin films and the CdS/CIGSe interface in a CdS thickness series, that has been sequentially prepared during the chemical bath deposition (CBD) process in dependence of the deposition time. We observe distinct features correlated to the CBD-CdS growth stages. In particular, we find that after an initial CBD etching stage, the valence band maximum (VBM) of the CIGSe surface is significantly shifted (by 180-620 mV) towards the Fermi level. However, VBM positions at the surface of the CIGSe are still much below the VBM of the CIGSe bulk. The CIGSe surface band gap is found to depend on the kind of post deposition treatment, showing values between 1.46 eV – 1.58 eV, characteristic for a copper-poor CIGSe surface composition. At the CdS/CIGSe interface a lowest VBM discontinuity is observed for the RbF-PDT sample. At this interface, a thin layer with a graded band gap is found. We also find that K and Rb act as compensating acceptors in the CdS layer. Detailed energy band diagrams of the CdS/CIGSe heterostructures are proposed.

1. INTRODUCTION

Recently, the light-to-power conversion efficiency of polycrystalline thin-film solar cells based on $Cu(In,Ga)(S,Se)_2$ (CIGSSe) absorber layers has been boosted to 23.35%.[1] This remarkable result was achieved after the introduction of an alkali-fluoride post-deposition treatment (PDT), e.g. initially by sodium-fluoride (NaF), of the $Cu(In,Ga)Se_2$ (CIGSe) absorber surface.[2] The application of a similar PDT procedure to the CIGSe absorber using fluorides of heavier alkali elements, e.g., potassium-fluoride (KF), rubidium-fluoride (RbF) and cesium-fluoride PDTs led to a series of record efficiencies in the past few years.[1,3-7] The application of alkali-PDTs in most of the studies resulted in absorber thin-films with improved bulk and surface electronic properties related to the alkali incorporation into the CIGSe (e.g., diffusion along grain boundaries and into grain interior[8,9] associated with the effects on the doping concentration, charge carrier life time and mobility)[10-14] and chemical changes of the thin-film top surface.[15] As already widely reported for most commonly used growth approaches, an untreated CIGSe thin-film surface has a Cu-depleted stoichiometry[16-18] which leads to a surface bandgap widening due to the downward shift of the valence band maximum (VBM) at a slight change of the position of the conduction band minimum (CBM). Such a surface band gap widening at the chalcopyrite thin-film absorbers is regarded as a crucial property for high-efficiency CIGSSe-based photovoltaic (PV) devices. However, along with this natural copper-depleted stoichiometry, the chalcopyrite thin-film surfaces show presence of sodium, which arises by diffusion from the applied soda-lime glass (SLG) substrates.[19-22] Moreover, on air-exposed, untreated (no PDT) absorber surfaces on SLG substrates Ga_2O_3, SeO_2, Na_xO, Na_2CO_3, and InO_x were observed.[8,21,23] Furthermore, treatment by different alkali elements led to formation of different surface phases.

For CIGSe exposed to a KF-PDT, surface phases such as GaF_3, $KInSe_2$, In_2Se_3 or In_2Se_3:K were deduced and a larger widening of the surface band gap to over 2.0 eV was reported along with the changes in positions of both CBM and VBM.[24-27] A common finding in these investigations is a further reduced Cu content at the absorber surface.[15] Note that presence of potassium and formation of potassium-containing phases is conditioned by the presence of a Cu-poor CIGSe surface composition.[26] For RbF-PDT samples, InO_x and GaO_x phases were found.[28-30] In addition NaF, RbF, $In(OH)_3$, GaF_3 and secondary phases of Rb-In-Se, and In_xSe_y:Rb,Na were detected.[28,29,31] Only a small downward shift of both CBM and VBM was found, while a minor change of the surface band gap from 1.46 eV to 1.51 eV was recorded.[23] The Cu content at the CIGSe surface was found to be reduced as in the case of the KF-PDT.

The subsequent growth of the CdS buffer layer on top of the CIGSe absorber by chemical bath deposition (CBD), in view of forming the active CdS/CIGSe heterojunction of the PV devices, is also influenced by the kind of absorber surface conditioning. During the CBD process, oxide phases as well as surplus NaF, KF and RbF are etched off from the CIGSe surface.[15,21,29,30] The etching effect is attributed to ammonia (NH_3), which is a constituent of the CBD solution. The CdS films grow denser and more homogeneously after the PDT treatment of the absorber surface.[31] Upon formation of the CdS/RbF-PDT CIGSe interface, the bands bend downward. However, a flat CBM alignment at approximately 0.51 eV from the Fermi level (E_F) was found between the CdS buffer and the RbF-PDT CIGSe layer.[23] A similar CBM alignment was found for the case of the CdS/CIGSSe interface.[32] The bandgap of the bulk CdS in the latter case was reported of 2.46 eV against 2.60 eV in the case of CdS grown on RbF-PDT CIGSe.[23] The former value is in agreement with the previously published data,[33-35] while the significantly

larger latter one is attributed to CdS with inclusions of $Cd(OH)_2$ and/or $CdSO_4$.[23] It was found in addition that Rb and Na atoms diffuse toward the CdS surface.[30]

The results reviewed above show an impressive work realized and a large amount of data collected. However, the full impact of the alkali-fluoride PDTs on the electronic structure of the CdS/CIGSe heterojunction used in solar cells and the correlation to their photovoltaic parameters are not yet fully understood. Moreover, due to the application of methods which require ultra-high vacuum, e.g., X-ray and UV photoelectron spectroscopy as well as inverse photoemission spectroscopy, the studies have been conducted on a limited number of samples. It is the aim of this work to determine the electronic parameters and propose detailed energy level diagrams for the CdS/CIGSe interface in high-efficiency solar cells based on PDT CIGSe absorber thin films using heavy alkali metal fluorides such as KF and RbF. For this purpose, we investigate (i) the impact of the KF-PDT and RbF-PDT on the electronic structure of the CIGSe layer and (ii) the CdS/CIGSe interface in a sequential time-dependent CdS thickness evolvement during the CBD process. We combine Kelvin probe (KP) and photoelectron yield spectroscopy (PYS) methods at ambient conditions to determine the work function (Φ) and the energetic position of the valence band maximum (E_{VBM}) of surfaces and interfaces. We complement the obtained Φ and E_{VBM} results by the data on the conduction band minimum energy (E_{CBM}) and propose, by considering the thin film band gaps obtained from internal quantum efficiency (IQE) measurements on solar cells, the detailed band diagrams. Finally, the obtained energy band diagrams are correlated to the PV parameters of the corresponding solar cells.

2. EXPERIMENTAL SECTION

2.1. Samples. In order to investigate the impact of the KF- and RbF-PDTs on the electronic properties of the CIGSe thin-film surface as well as the formation of the CBD-CdS/CIGSe interface during the growth of the CdS buffer layer in dependence of the CdS thickness, three sample sets (10 pieces each) for (i) no-PDT (ii) KF-PDT and (iii) RbF-PDT respectively were made from CIGSe thin-films deposited by otherwise nominally identical fabrication processes. The CIGSe thin-films were prepared by a three-stage co-evaporation process[36] on 1 mm thick SLG substrates coated with 400 nm thick DC-sputtered molybdenum.[31] The SLG substrates were used without a diffusion barrier coating, so that Na can diffuse from the substrates into the CIGSe films during growth. The integral composition, as measured by X-ray fluorescence spectroscopy (XRF), exhibited $x_{Cu}/(x_{Ga}+x_{In}) = CGI \approx 0.80$ and $x_{Ga}/(x_{Ga}+x_{In}) = GGI \approx 0.35$, x denoting the molar fraction of the respective element. Details about the CIGSe deposition process can be found elsewhere.[31,37] After the CIGSe deposition, the samples for the second and third sets were immediately transferred through air to vacuum deposition tools for the KF-PDT and RbF-PDT treatments. Both PDTs consisted of evaporating the respective alkali-fluoride at rates between 0.1-0.2 Å/s under Se atmosphere at substrate temperatures between 280-350°C for 15 minutes.[26,31] One sample from each of the three sets was kept as reference for further investigations. The subsequent CdS deposition on the other samples was performed in an aqueous CBD solution consisting of Cd-acetate [2.6 mM], thiourea [0.1 M] and ammonia [1 M] at 58°C.[31] To avoid cross-contamination, the untreated, KF-treated, and RbF-treated samples were immersed in separate glass beakers. The time counting was started immediately after the samples' immersion and, starting after 1 min, one sample was taken out of the bath per minute resulting in a variation of the CBD-duration from 0 min to 9 min. The XRF data show that CdS deposition starts at 1.8 ± 0.3 min, 1.7 ± 0.3 min and 2.3 ± 0.4 min for the no-PDT, KF-PDT and

RbF-PDT samples, respectively (see Figure S1). The growth rates determined for the deposition time between 3–7 min achieve 6.6 ± 1.0 nm/min, 7.8 ± 1.2 nm/min and 7.0 ± 1.8 nm/min for the no-PDT, KF-PDT and RbF-PDT samples, correspondingly. The thin-film thicknesses after 9 min CBD deposition time are: 42 ± 6 nm, 48 ± 5 nm, 49 ± 6 nm for the no-PDT, KF-PDT and RbF-PDT treated CIGSe absorbers, respectively. All samples were stored in a vacuum desiccator and air-exposure was kept to a minimum. Further details on these samples and a detailed discussion of the CdS growth on the differently treated CIGSe surfaces can be found here.[31] The KP-PYS measurements were conducted on single samples after being removed from the desiccator.

2.2. Characterization methods. The KP[38,39] and the PYS[40-42] methods were combined in an ambient pressure KP Technology SKP5050-APS02 instrument[43,44] to determine the materials surface electronic properties such as the work function, Φ, and the ionization energy (E_i). The advantage of combining these methods is that (i) the same tip electrode is used as the current collector and (ii) the work-function of samples, including that of the reference sample for KP measurements, can be directly checked by the PYS measurements which are independent of the Φ_{tip}.

Kelvin Probe. The KP method for determining the materials work-function is based on measuring the contact potential difference (CPD) between the Kelvin probe as reference (Kelvin electrode) and the investigated sample. The CPD can be found by compensating it by an external dc bias voltage (V_{dc}) until $V_{CPD} + V_{dc} = 0$. Since $-e \cdot V_{CPD} = \Phi_{tip} - \Phi_{sample}$, where e is the elementary charge, with the known Φ_{tip} the work function of the investigated sample is calculated. The precise determination of the V_{CPD} is based on measuring the ac current (i_{ac}) which flows through the capacitor (formed between the Kelvin electrode and the investigated sample) if the distance

between the two plates is harmonically varied.[45-48] The dependence of the i_{ac} on the modulation of the capacitance was analyzed in terms of a simple equivalent circuit (Figure S2a) in which the built-in potential, V_{CPD}, is represented as a battery which is connected in series with an external battery of an adjustable dc bias, V_{dc}. For the actual measurements of the V_{CPD}, an additional null-current detector is inserted in series in the circuit. Then, for a certain voltage ($V_{CPD} + V_{dc}$) and a change in capacitance due to the Kelvin electrode's oscillation, the current is given by $i_{ac}(t) = (V_{CPD} + V_{dc})\,(dC(t)/dt)$. In this equation, the capacitance $C(t)$ of the capacitor with two parallel plates of an area A varies due to the variable distance $d(t) = d_0 + d_1 \cdot sin(\omega t)$, where d_0 is the capacitor mean spacing and d_1 is the amplitude of oscillation with the angular frequency ω. The voltage V_{dc} is changed until the null-current condition in the circuit is detected by a sensitive current amplifier within the null-method approach. This compensating voltage $V_{dc} = - V_{CPD}$ is recorded as the contact potential difference between the two plates of the capacitor. Another approach of recording the V_{CPD} is based on the off-null detection method[44,49] which uses the dependence of the peak-to-peak output voltage (V_{ptp}) on V_{dc} since the V_{ptp} is proportional to ($V_{CPD} + V_{dc}$). In this case, the V_{CPD} is determined from the intercept of the $V_{ptp} = f(V_{dc})$ curve at $V_{ptp} = 0$ V from two high-signal level measurements (Figure S2b). The determined gradient (slope) $G = \Delta V_{ptp}/\Delta V_{dc}$ is used in a feedback control loop to maintain a constant mean tip-to-sample distance, i.e., the probe to sample spacing can be controlled by pre-setting G.

The KP system used in this study employs a 2.0 mm diameter tip with a gold-alloy coating. In the CPD mode, the tip is vibrated at 75 Hz with an amplitude of approximately 0.2 mm at a pre-set gradient $G = 300$ resulting in an average tip-sample spacing of about 1.0 mm. The KP setup is placed in a Faraday cage which screens the eventual external electrical fields and allows for a controlled sample illumination. The samples with the size of up to 5×5 cm^2 are mounted on

a motorized 3-axis stage with a transitional position control of <300 nm which allows for selective as well as mapping options. Reference measurements for the calibration of the work function of the tip, Φ_{tip}, were conducted on an Au thin-film. Typical Φ_{tip} values between 4.92 eV – 5.00 eV were determined by means of the photoelectron yield spectroscopy (see next chapter). Subsequently, the work function of the sample, Φ_{sample}, was calculated from the CPD data according to $\Phi_{sample} = \Phi_{tip} + e \cdot CPD$. The measurements of the surface photovoltage (SPV)[50] defined as $SPV = CPD_{light} - CPD_{dark}$ were performed using laser diodes with wavelength/energy of 405 nm/3.06 eV, 450 nm/2.75 eV, 532 nm/2.33 eV, 670 nm/1.85 eV, and 980 nm/1.26 eV with a light power density of ~100 mW/cm^2. The CPD resolution, as determined on an Au thin film, is better than 2 mV (see Figure S3). The standard CPD deviation depends yet on the material surface state and was therefore determined in each measurement separately.

Photoelectron yield spectroscopy. The PYS method was first established in vacuum[41,42,54] and then steadily developed for the application in non-vacuum ambiance, e.g., in air.[43,44,51-56] The photoemission process in vacuum consists of the following steps: (i) optical excitation of electrons into states of higher energy, (ii) electron transport towards the surface, and (iii) escape through the surface to vacuum.[57] During the steps (ii) and (iii), primary photoelectrons are inelastically scattering and secondary electrons with lower kinetic energies are excited. For the low kinetic energy electrons an escape depth <50 Å was reported.[42,54] The escaped electrons are easily collected under the application of a moderate electrical field in order to avoid the formation of the negative space charge near the sample surface. Under ambient conditions, an ionic current is recorded instead of an electronic one. In air, the ejected electrons with a mean free path of less than 1 µm attach to the air constituent molecules and form anions such as O_2^-,

N_2^- and OH^-.[44,55,61] Having a much higher mean free pass than the electrons, these anions drift to the positively charged electrode, thus allowing to record the photoelectron current indirectly.

The PYS method for determining the work-function of metals and the ionization energy of semiconductors is based on measuring the photoelectron yield $Y(h\nu)$ as a function of photon energy $h\nu$, $Y(h\nu)$ being defined as the number of photoemitted electrons per incident photon, at a given photon energy $h\nu$. If the photon energy becomes greater than the threshold ionization energy, E_i, the $Y(h\nu)$ value starts to increase according to

$$Y(h\nu) \propto (h\nu - E_i)^n. \quad (1)$$

The power index n = 2 for metal samples[58] and degenerate semiconductors. For most of inorganic semiconductors n = 3 when considering the volume excitation,[59] while n = 1, 3/2, 5/2 depending on the contribution of the surface imperfection and band states.[60,61] For a large number of organic materials n = 3 is observed,[62] as in the case of inorganic semiconductors. Thus, the E_i value is determined as the threshold in the $h\nu - Y^n$ plots. In addition to the ionization energy, the PYS spectra contain the information on the effective density of states spreading from the Fermi level (E_F) down to $h\nu$ - Φ below E_F.[41]

In our work, the PYS setup uses the same Kelvin probe (static) to detect the photoemission currents as a function of the incident photon energy. The light source comprises a deuterium (D_2) lamp coupled with a grating monochromator. The range of the incident photon energy is 3.4-7.0 eV. The light is guided via a DUV optical fiber forming on the sample surface an elliptical spot with a size of approximately 3 × 4 mm^2. A bias potential of +10 V is applied to the tip. The photoemission threshold is determined with a resolution of 30 meV.

The information depth (ID) of the PYS measurements is estimated by considering the exponential attenuation of photoelectrons in matter according to the kinetic energy-dependent inelastic mean free paths (IMFPs) (see Figure S4 and related explanations). Thus, if photoelectrons are detected as generated at a distance of 3×IMFP below the sample's surface, the signal will be attenuated to 5%. Therefore, the ID of our PYS measurements is estimated to approximately 3×IMFP, and hence, the PYS spectra measured from closed layers with thicknesses exceeding 3×IMFP can be accurately recorded without being influenced by the substrate. The ID values were estimated for Cu, In, Cd, Se and Na electrons. The highest ID of approximately 3.8 ± 0.8 nm is found for In electrons. The maximum values of IDs for Cu, Cd and Se may be approximated to 1.2 ± 0.3 nm, 1.5 ± 0.3 nm, and 1.4 ± 0.3 nm, respectively. The ID for Na is 2.1 ± 0.4 nm. Thus, the conducted PYS measurements will not record any contribution from the CIGSe substrate after its coverage by a continuous layer with a thickness >3.8 nm. The PYS spectra from subsequently deposited films which contain Cd will be measured with an ID of approximately 1.5 nm.

2.3. Evaluation of electronic parameters. As the measurements were performed in ambient conditions, assumptions are made concerning possible surface dipoles due to air exposure. (i) Molecules adsorbed from air, e.g., oxygen and/or adventitious hydrocarbon (C-C, C-H bonds) promote formation of a surface dipole ($\Delta\phi_s$) (see Figure S5), called thereafter the "adsorbed surface dipole", on both sample and tip surfaces thus resulting in no influence to the measured *CPD* and, consequently, to the calculated work function values (since the $\Phi_{sample} = \Phi_{tip} + e \cdot V_{CPD}$). (ii) The sample surface is chemically stable during the short time exposure to the ambience so that the native oxides potentially present at the film surface and thus the related

"native surface dipole" show no or negligible development. If these assumptions are fulfilled, the results obtained under the ambient measurement conditions shall agree well with the Φ and E_i values obtained by measurements conducted under non air-exposed conditions, e.g., in vacuum. Notice that for each measured surface, Φ defines the local vacuum level (see Figure S5). The VBM development relative to the Fermi level, E_F, can be then found as

$$E_{VBM} = \Phi - E_i. \quad (2)$$

For measurements in the dark, the E_{VBM} includes the surface band bending contribution as comprised in Φ. The band bending can be eliminated, if the Fermi level at the surface is not pinned, by performing KP measurements under sufficiently intense illumination with photons of energies higher than E_g. Thus, for the obtained E_{VBM} the bulk values may be assumed if the contribution of the native surface dipole is neglectable. With the E_{VBM} data, the CBM development can be calculated as $E_{CBM} = E_{VBM} + E_g$ by considering the E_g values obtained from complementary measurements and literature data. The complementary measurements include photoelectron yield spectra on reference samples and quantum efficiency measurements on complete solar cells.

3. RESULTS AND DISCUSSION

The results of the work function measurements performed in the dark on no-PDT, KF-PDT and RbF-PDT conditioned CIGSe samples as a function of the CdS chemical bath deposition time (t_{CBD}) are presented in Figure 1. The measured work functions of all samples show time-dependent variations within standard deviations of ±15 meV to ±26 meV around constant mean

values confirming the validity of the assumption made regarding the surface chemical stability. Higher standard work function deviations compared to that of the Au reference could be a hint for electronic inhomogeneities at the sample's surface as reported earlier.[63] The averaged work function data for these measurements are plotted as a function of the CBD-CdS deposition time in Figure 1d. The graphs clearly depict the electronic state of the (i) bare CIGSe sample surface, which was not exposed to the CBD, i.e., at t_{CBD} = 0 min, (ii) CIGSe surface after an initial CBD

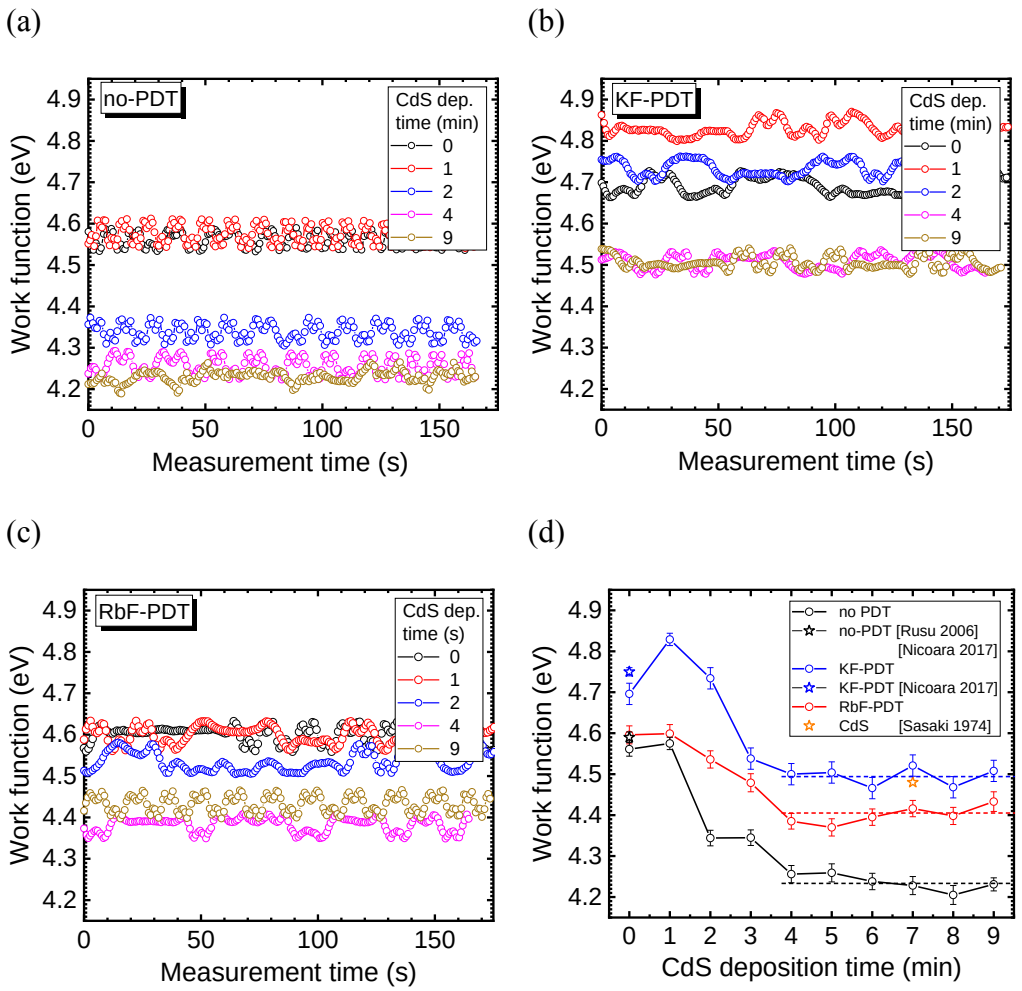

Figure 1. (a-c) Selected time dependent work function curves of the (a) no-PDT, (b) KF-PDT and (c) RbF-PDT conditioned CIGSe surface as a function of the CdS chemical bath deposition (CBD) time

shown in the inset. (d) Work function dependences of the no-PDT, KF-PDT and RbF-PDT conditioned CIGSe surface as a function of the CBD-CdS deposition time. The error bars show standard deviations determined in each individual KP measurement. Reference data from literature are shown for comparison.

stage of t_{CBD} = 1 min, (iii) CdS/CIGSe interface during 1 min ≤ t_{CBD} ≤ 4 min and (iv) CdS layer during 4 min ≤ t_{CBD} ≤ 9 min. The surface of the no-PDT sample shows a value of 4.56 eV which is close to the data published on CIGSe samples measured by the Kelvin probe force microscopy (KPFM).[12,64] The KF-PDT leads to a significant Φ increase by 140 meV up to 4.70 eV, in close agreement with the values published by Nicoara *et al.*[12] RbF-PDT however leads to a value of 4.60 eV which is very close to that of the no-PDT reference sample. The work functions of these samples remain almost at the same level also after 1 min immersion in the CBD bath. In contrast, the work function of the KF-PDT sample increases strongly to 4.83 eV, a value which is by 130 meV higher than that of the RbF-PDT treated CIGSe surface and by 250 meV greater compared to the no-PDT sample. The increase of the CBD-CdS deposition time up to 4 min leads to a continuous Φ decrease. Such a behavior of the work function correlates with the behavior of the CPD in KPFM studies on Rb-PDT CIGSe absorbers.[63] The achieved work function values of 4.23.eV, 4.41 eV and 4.49 eV for the no-PDT, RbF-PDT and KF-PDT, respectively, are close to values published in literature for CdS single crystals.[65] After 4 minutes, a further increase of the CBD-CdS deposition time results only in slight Φ fluctuations around the latter values.

The work function measurements were also performed under illumination. However, insignificant changes compared to the dark measurements were observed, which we explain by Fermi level pinning at the films surface.

The ionization energy of the CIGSe and CdS/CIGSe samples was determined by linear regression and extrapolation of the $Y^{1/3}(h\nu)$ spectra as shown in Figure 2 and summarized in

Figure 3a as a function of the CdS deposition time. As in the case of the evolution of the work function in Figure 1d, the same stages are observed for the E_i development. However, while the work function changes refer to variations in the Fermi level, the ionization energy variations denote surface chemistry changes. Notice that the E_i change in Figure 3a shows a minimum at t_{CBD} = 1 min. To understand such a behavior, we correlate the ionization energy development with the CBD-CdS deposition stages: (i) CIGSe surface etching.[15,21,29,30] (ii) Induction/coalescence process

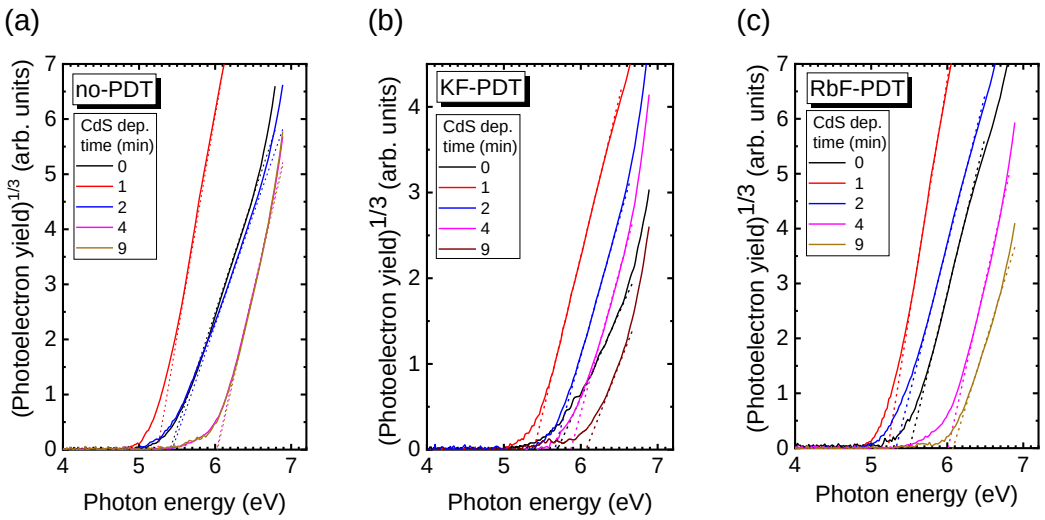

Figure 2. Selected photoelectron yield spectra (PYS) of the (a) no-PDT, (b) KF-PDT and (c) RbF-PDT conditioned CIGSe surface as a function of the CdS chemical bath deposition time shown in the insets. The dashed lines represent linear fittings extrapolated to the photon energy axis for defining the ionization energies.

(a) (b)

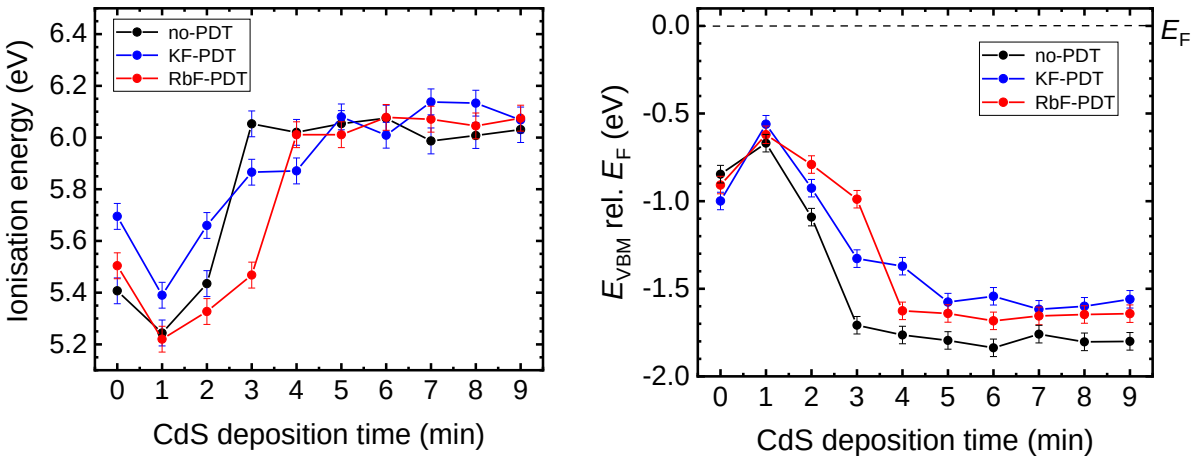

Figure 3. (a) Ionization energy dependences of the no-PDT, KF-PDT and RbF-PDT conditioned CIGSe surface as a function of the CBD-CdS deposition time. The error bars indicate the error margin of ±30 meV of the PYS setup. (b) Valence band edge (E_{VBM}) relative to the Fermi level (E_F) of the no-PDT, KF-PDT and RbF-PDT conditioned CIGSe surface as a function of the CdS chemical bath deposition time. The error bars are mean root square errors derived from respective errors of the work function and ionization energy.

associated with the $Cd(OH)_2$ adsorption. Notice that during this stage no CdS is deposited and that its duration depends strongly on the chemical structure of the surface and its morphology.[31,66] (iii) The ion-by-ion CdS growth and (iv) cluster-by-cluster deposition.[66,67] Thus, the first CBD stage can be depicted for a duration of up to 1 min, followed by a second stage for the duration 1 min ≤ t_{CBD} ≤ 3(4) min and by the third CBD stage for the duration 3(4) min ≤ t_{CBD} ≤ 9 min. The fourth CBD stage seems to have a minor contribution for the t_{CBD} ≤ 9 min since no essential changes in the ionization energy are observed. Therefore, this last CBD stage will be omitted from further discussions. Thus, by applying the above correlation, we claim that the specific minimum of the ionization energy at t_{CBD} = 1 min may be assigned to the end phase of the CBD etching process of the CIGSe surface. The t_{CBD} = 1 min time is found below the starting time of the CdS growth between 1.7–2.3 min (see Experimental Section) which

appears reasonable when considering the second induction/coalescence deposition stage. Above this time, as can be seen on the graph in Figure3a, the ionization energies achieve values characteristic of thick CdS films at about 3 min for no-PDT and 4–5 min for RbF-PDT and KF-PDT samples. The PYS spectra in Figure 2 and their enlarged versions in Figure S6 show no signatures from the CIGSe substrate for the times found for RbF-PDT and KF-PDT, meaning that the CdS thickness is at least above the ID related to In electrons, i.e., of 3.8 ± 0.8 nm. For the no-PDT sample at 3 min deposition time, the PYS spectrum still shows a contribution from the CIGSe substrate (see Figure S6a). We correct therefore the time corresponding to the PYS information depth for CIGSe to 3.5 min (with an error of approximately ±0.5 min), corresponding to a CdS capping layer thickness of 11.2 ± 1.6 nm. Thus, we find an experimental information depth for the PYS measurements on CIGSe thin-films of 11.2 ± 1.6 nm, in good agreement with the ID found for In electrons.

The surface ionization energy of the reference no-PDT sample (corresponding to t_{CBD} = 0 min in Figure 3a) amounts to 5.41 eV. An E_i = 5.50 eV close to the latter value is observed for the RbF-PDT sample, while the ionization energy of the KF-PDT sample significantly increases to 5.70 eV. In the case of the KF-PDT treated CIGSe surface, the E_i = 5.70 eV lies between values of 5.60 eV and 5.84 eV measured on the reference In_2Se_3 thin films deposited on Mo/SLG and SLG substrates, correspondingly (see Figure S7). This result points to the formation on the KF-treated CIGSe surface of an In_2Se_3 phase (with a bandgap of 2.0 eV),[68] which is in agreement with previous studies that have reported presence of K-In-Se and In_2Se_3:K surface phases.[25,26] The surface E_i = 5.50 eV of the RbF-PDT CIGSe reference is close to 5.41 eV of the no-PDT reference sample with the Cu-poor surface composition. Moreover, after the CBD surface etching stage the ionization energy of the RbF-PDT and no-PDT samples, 5.22 eV versus 5.24

eV, practically coincide within the error bars. It can be thus concluded that in both cases the CIGSe surface has a similar Cu-poor surface composition. The deviations in E_i for the RbF-PDT sample may be attributed to the effects of Rb on the CIGSe surface chemistry and electronics. Note that after a RbF-PDT a surface band gap of 1.51 eV was found on CIGSe thin films[23] which fits to the bandgaps of the Cu-poor surface composition between 1.4 eV for $CuInSe_2$[18] and 1.61 eV for $Cu(In,Ga)Se_2$.[24] In spite of the large E_i values observed on bare CIGSe samples, after 1 min dipping in the CBD solution, the E_i of all samples decreases significantly, as previously observed, to 5.24 eV, 5.22 eV and 5.39 eV for the no-PDT, RbF-PDT and KF-PDT samples, accordingly. These ionization energy changes indicate chemical modifications of the surface of the thin films agreeing with the etching effects of the CBD mentioned above.[15,29,30] The significant decrease of E_i is followed by a gradual increase of the ionization energy of all samples for the deposition times up to 3-4 minutes. This indicates a gradual change in the physico-chemical properties of the samples surface, which we attribute to the nucleation of the $Cd(OH)_2$ molecules on the CIGSe surface during the induction/coalescence phase of the CBD-CdS growth process[66,67] and to the diffusion of Cd-atoms into the chalcopyrite lattice creating Cd_{Cu} anti-sites from the available Cu vacancies, V_{Cu}.[31,69] We emphasize that there might be more complex reactions taking place on a smaller time scale than we probed, e.g., formation of CdSe at 1 s CBD immersion time.[63] Note however that no CdSe was detected for any of the CBD-CdS deposition times >1 s investigated here.[63] The further increase of the CBD-CdS deposition time results in a value of about 6.05 ± 0.03 eV for all samples. The fluctuations observed are explained by slightly different surface dipoles on different samples. The latter E_i value coincides in fact within the error bars with the one measured on CdS reference layers prepared by the same

CBD process on ITO/glass substrates (Figure S8). Thus, for the CBD-CdS deposition times >4 min closed CdS films with similar chemical properties are prepared independently of the PDT.

Using the work function data in Figure 1d and the ionization energy results in Figure 3a, the development of the VBM at the CdS/CIGSe interface relative to the Fermi level is plotted in Figure 3b (according to the equation 2). The fluctuations of E_{VBM} are reduced compared to the variations observed for the work function and ionization energy, since for each pair of Φ and E_i data the specific local vacuum level is used. Thus, the influence of the native surface dipole is excluded (consult Figure S5). The VBM values of -0.85 eV, -0.91 eV and -1.18 eV for the no-PDT, RbF-PDT and KF-PDT reference samples, respectively, are similar within the error bars to the published data.[23,24,27] After 1 min immersion of samples in the CBD-CdS solution, the VBM positions change significantly to values of -0.67 eV, -0.62 eV and -0.56 eV for the no-PDT, RbF-PDT and KF-PDT samples, correspondingly. Good agreement with the available data is found for the KF-PDT sample.[24] The E_{VBM} = -1.79 eV of a thick CdS thin film deposited on a no-PDT CIGSe sample is found in good agreement with the literature data.[23,32]

Considering the obtained VBM graphs in Figure 3b, we now plot the CBM edges in Figure 4 by considering the relation $E_{CBM} = E_{VBM} + E_g$. The respective bandgaps are considered based on the chemical and electronic structure of the CIGSe surface state as well as the CBD-CdS deposition phases. The following scheme related to the CBD deposition time, t_{CBD}, is applied:

- t_{CBD} = 0 min & PDT-CIGSe surface: E_g of the no-PDT, KF-PDT and RbF-PDT CIGSe as identified from literature by comparing the surface chemical composition and electronic properties which fit to our data, e.g., to E_{VBM} results.
- t_{CBD} = 1 min & CBD-etched CIGSe surface: available E_g values for the Cu-poor surface composition after the CBD etching phase.

- t_{CBD} = 2 min & beginning of the CBD induction/coalescence regime (initiation of the $Cd(OH)_2$ nucleation): E_g which results from considering the measured in this work VBM position and the same E_{CBM} as for the t_{CBD} = 1 min, since a flat band CBM alignment was determined at the CIGSe/CdS interface in most of the studies conducted on the overall Cu-poor CIGSe thin films.[23,32]
- 2 min ≤ t_{CBD} ≤ 3(4) min & CBD-CdS induction/coalescence regime ($Cd(OH)_2$ nucleation): graded E_g resulting from the VBM and CBM changes. Note that during this CBD phase, with a duration dependent on the substrate surface condition, no CdS was found.[31,67]
- 3(4) min ≤ t_{CBD} ≤ 9 min & CBD-CdS ion-by-ion growth regime:[66,67] $E_{g\text{-}CdS}$ = 2.42 ± 0.02 eV as determined from internal quantum efficiency measurements on complete solar cells. We consider here the constant E_g being aware of the fact that at a longer CBD duration the CdS ion-by-ion growth phase may have been complemented by the cluster-by-cluster (colloidal) growth regime, which still however does not show a visible influence on the CdS opto-electronical properties.

A summary of the considered and calculated data is presented in Table 1.

The obtained results for the VBM and the CBM development as a function of the CBD-CdS deposition time are presented in Figure 4 for each PDT separately. For the sample with no-PDT in Figure 4a, we assume a surface band gap of 1.46 eV corresponding to a Cu-poor, vacancy compound or reconstructed surface, in accordance with Hauschild *et al.*[23] For the cleaned surface - after 1 min CBD - the same surface E_g is considered as that is attributed to the same Cu-poor surface composition as in the previous case, however after oxide removal. The oxide removal is electronically equivalent to the surface dipole removal, thus shifting

both the VBM and CBM edges upward without changing E_g. The CBM position at the beginning of the $Cd(OH)_2$ nucleation phase, i.e. for the 2 minutes CBD duration, is still kept constant at the level of the cleaning stage since for the CdS/CIGSe interface a flat CBM band alignment was reported.[23,32] Note that there are numerical simulation studies as well as some experimental

Table 1. VBM, CBM and Electronic Surface Band Gap Energies of the no-PDT, KF-PDT and RbF-PDT CIGSe Absorbers and CIGSe/CdS Interface after Different CBD Duration[§]

CIGSe	no-PDT			KF-PDT			RbF-PDT		
CBD duration (min)	E_{VBM} (eV)	E_{CBM} (eV)	E_g (eV)	E_{VBM} (eV)	E_{CBM} (eV)	E_g (eV)	E_{VBM} (eV)	E_{CBM} (eV)	E_g (eV)
0	0.61 ± 0.05	0.85 ± 0.12	1.46 ± 0.11[23]	1.18 ± 0.05	0.82 ± 0.06	2.0 ± 0.1[68,a]	0.91 ± 0.05	0.60 ± 0.12	1.51 ± 0.11[23]
1	0.67 ± 0.05	0.79 ± 0.12	1.46 ± 0.11[23]	0.56 ± 0.05	1.02 ± 0.12	1.58 ± 0.30[24]	0.62 ± 0.05	0.89 ± 0.12	1.51 ± 0.11[23]
2	1.09 ± 0.05	0.79 ± 0.12	1.88 ± 0.13	0.93 ± 0.05	1.02 ± 0.12	1.95 ± 0.13	0.79 ± 0.05	0.89 ± 0.12	1.68 ± 0.13
3	1.71 ± 0.05	0.71 ± 0.05	2.42 ± 0.07	1.52 ± 0.05	0.86 ± 0.05	2.38 ± 0.07	0.99 ± 0.05	0.80 ± 0.05	1.79 ± 0.07
4 – 9	1.79 ± 0.05	0.63 ± 0.05	2.42 ± 0.02[b]	1.59 ± 0.05	0.83 ± 0.05	2.42 ± 0.02[b]	1.64 ± 0.05	0.78 ± 0.05	2.42 ± 0.02[b]

[§] E_{VBM} data are derived from our KP-PYS measurements. The E_{CBM} values are determined as $E_{VBM} + E_g$ except those for the 2 min CBD duration. The E_{CBM} values for the latter CBD duration were assumed similar to those at t_{CBD} = 1 min since most of studies performed by photoelectron spectroscopy measurements have found a flat band CBM alignment at the CdS/CIGSe interface (with Cu-poor CIGSe surface composition).[23,32] The E_{CBM} data for t_{CBD} = 3 min is determined from extrapolated values between the CIGSe surface at t_{CBD} = 2 min and the formed CdS thin film at t_{CBD} = 4 min. The resultant band gaps were then accordingly calculated.
[a]Band gap of the identified In_2Se_3 thin film in our PYS measurements.
[b]Band gap of CdS thin films determined from internal quantum efficiency measurements on complete ZnO/CdS/CIGSe/Mo/SLG solar cells.[31]

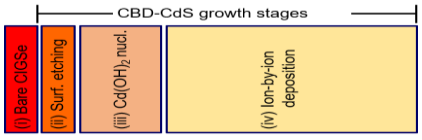

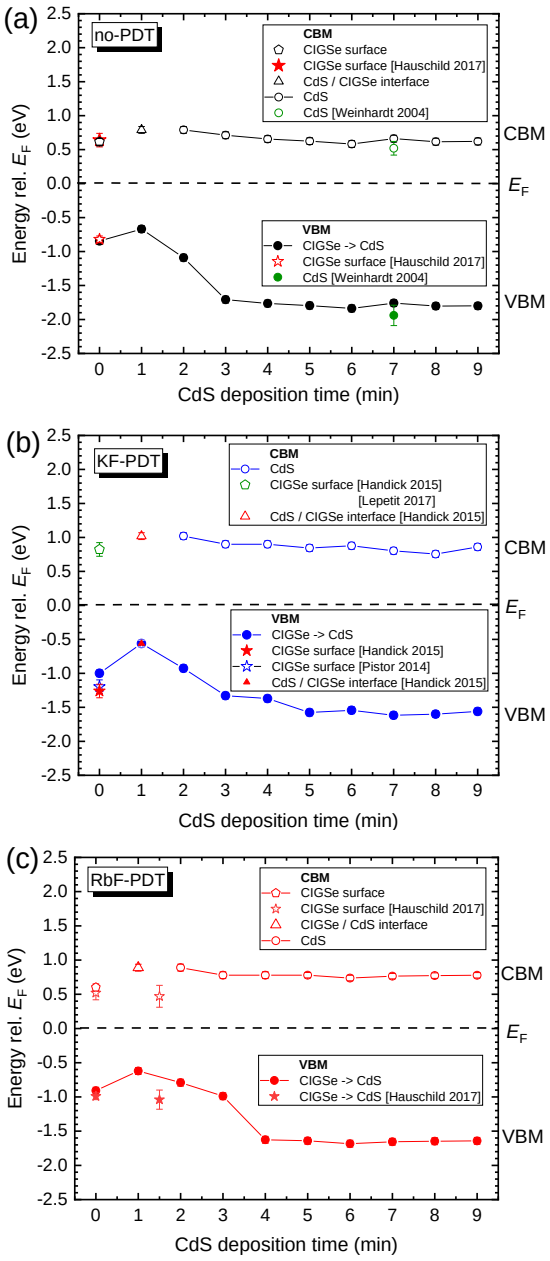

Figure 4. Evolution of the valence and conduction band edges (VBM, CBM) of the (a) no-PDT, (b) KF-PDT and (c) RbF-PDT conditioned CIGSe surface.

findings that report a spike-like CBM alignment at the abrupt absorber/buffer interface.[70,71,72] For this CBD deposition time, however, the CdS growth still does not occur, as concluded above. Since the VBM shows constant values starting from approximately 3 min CdS deposition time,

we consider this time point as the beginning of the ion-by-ion growth phase of the CdS layer[31,67] with an $E_{g\text{-}CdS}$ = 2.42 ± 0.02 eV determined from corresponding internal quantum efficiency measurements on solar cells.[31] For the bare KF-PDT reference sample, a surface band gap of 2.0 eV is considered based on our PYS results, which suggest the presence of an In_2Se_3:Na layer, and reports in literature that have proposed an In_2Se_3:K layer at the CIGSe surface.[24-27] For the cleaned surface after 1 min CBD, a minimum surface band gap of 1.58 eV is considered, as reported by Handick *et al*.[24] (being aware that these reference data are taken from films prepared by a low-temperature multistage process on molybdenum coated polyimide foils). We note that, as in the case of no-PDT, the CBM position at the beginning of the $Cd(OH)_2$ nucleation phase (i.e., for the 2 min CBD duration) is kept at the same level. Starting from approximately 3 min of the CdS deposition, a constant $E_{g\text{-}CdS}$ = 2.42 eV is considered. In the case of the RbF-PDT reference sample, a surface band gap of 1.51 eV is assumed, as determined by Hauschild *et al*.[23] The same surface E_g is presumed for the cleaned CIGSe surface after 1 min of the CBD processing, resulting in a E_{CBM} = 0.89 eV. This latter value is assumed also for the CBM position at the beginning of the CdS induction/coalescence phase, i.e. at 2 min of the CBD-CdS deposition time. For the ion-by-ion CdS growth phase, an $E_{g\text{-}CdS}$ = 2.42 eV is considered, as in the previous cases.

From the above findings of the behaviour of the work function, ionization energy, the VBM and CBM positions, we conclude that the initial surface state of the no-PDT, KF-PDT and RbF-PDT samples, characterized by large VBM downward shifts, is not preserved after the immersion in the CBD-CdS solution. Due to the etching effect of ammonia during the first CBD minute, the CIGSe surface is cleaned from oxides and simultaneously from K-In-Se and Rb-In-Se phases formed during the KF-PDT and RbF-PDT. That is why the E_{VBM} of the CIGSe surface

changes to values between 0.56 eV – 0.67 eV. The observed differences in the E_{VBM} are attributed to doping by the K and Rb atoms diffused into the Cu-poor CIGSe surface layer. Thus, because during the CBD etching stage surface phases are removed from CIGSe, we will consider in the final band diagrams the electronic states of the CIGSe layers as after the 1 min immersion in the CdS chemical bath.

In the final energy band diagrams, we will consider in addition the CIGSe thin-film bulk band gap of 1.18 eV determined from internal quantum efficiency measurements on solar cells prepared from identically processed absorbers.[31] The VBM position relative to the Fermi level is found according to Fermi-Dirac statistics[73] by considering the density-of-state effective mass for holes in CIGSe $m_p = 0.235m_0$,[74] where m_0 is the electron rest mass, and the concentration of holes of 1.1×10^{16} cm^{-3} determined from capacitance-voltage measurements on accompanying solar cells made from the same absorbers. We thus obtain the $E_F - E_{VBM} = 0.14$ eV.

The VBM and CBM of the CIGSe bulk are shown in Figure S9 along with the surface electronics immediately after the respective PDTs and the changes that occurred after 1 min CBD duration. We note that the VBM of the CIGSe surface is still much lower than the VBM of the CIGSe bulk, however not as low as immediately after the PDT process. Considering this CIGSe bulk/surface energy level structure and completing it by the VBM and the CBM development for the CBD duration ≥1 min from Figure 4, we propose detailed energy band diagrams in Figure 5. We observe features which were not previously reported. The CIGSe surface band gap varies, depending on the kind of conditioning, from 1.46 eV to 1.51 eV and 1.58 eV for the no-PDT, RbF-PDT and KF-PDT, respectively (see also data for 1 min CBD duration in Table 1). This may be a hint for different effects of the Na, Rb and K on the electronic properties of the Cu-poor CIGSe surface layer due to the in-diffusion of those species.

At the CIGSe/CdS interface the lowest VBM-discontinuity of 0.17 eV is observed for the RbF-PDT sample. That could be an indication for beneficially lower saturation currents of illuminated solar cells. In addition, at the CIGSe/CdS interface a gradual change of the band gap between the CIGSe surface and the CdS thick layer is observed. Thus, interfacial band gaps of 1.88 eV, 1.95 eV and 1.68 eV are observed for no-PDT, KF-PDT and RbF-PDT, respectively. These band gaps increase then gradually to the band gap of CdS thick layer of 2.42 eV. Hence, the highest band gap gradient, related mostly to the VBM variation, is observed for the RbF-PDT sample. We attribute this gradual increase of the interfacial band gap to a continuous change in the CdS thin film composition. The differences observed for the starting band gaps can be explained by differences in the starting layer stoichiometry influenced by the CIGSe absorber surface chemistry. This interfacial model is supported by the data on the [Cd]:[S] ratio of about 3:1 reported for 1–5 min CBD deposition time.[63] The previously estimated CdS thickness for the capping layer on no-PDT sample of about 11 nm may be attributed to such an interfacial layer. For the RbF-PDT and KF-PDT samples we find interfacial layer thicknesses of ~12 nm and ~18 nm, respectively. Thus, we propose that, due to compositional changes, the band gap of the growing CdS buffer layer gradually changes from non-stoichiometric to stoichiometric CdS within the formation of the first 11–18 nm of the buffer. Note that the contribution of the OH groups and alkali, C or In atoms[26,63] is not excluded. For the thick CdS layer we observe that the CBM positions of the KF-PDT and RbF-PDT samples shift upward compared to the no-PDT sample which shows the lowest E_{CBM}-E_F = 0.63 eV. The E_{CBM}-E_F increases to 0.78 eV for the RbF-PDT and to 0.83 eV for the KF-PDT samples. The increased E_{CBM}-E_F of CdS layers point at a decreased charge carrier concentration. The magnitude of

(a)

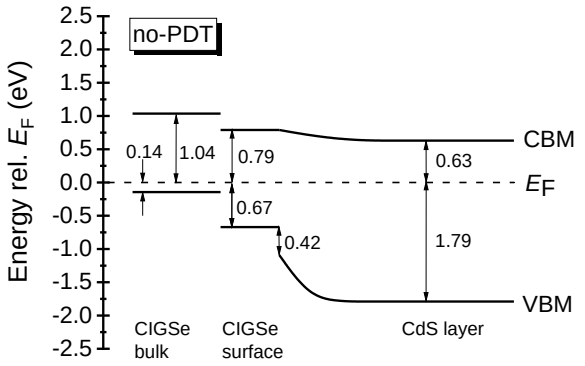

(b)

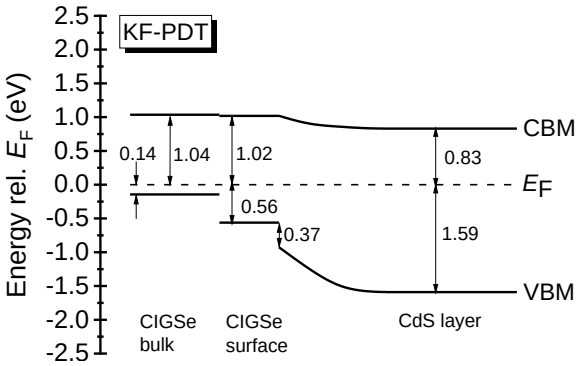

(c)

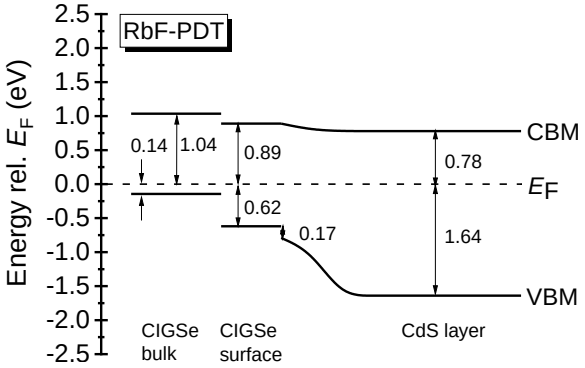

Figure 5. Energy band diagrams of the CIGSe/CdS heterojunction with (a) no-PDT, (b) KF-PDT and (c) RbF-PDT conditioned CIGSe surface.

variations in charge carrier concentration are found from estimations on the CdS surface. By applying the Fermi-Dirac statistics for the n-type CdS with the $m_n = 0.25m_0$[75] and using the E_{CBM}-E_F values, we obtain the concentration of the free electrons on the CdS surface of 8.2×10^7 cm^{-3}, 2.5×10^5 cm^{-3} and 3.6×10^4 cm^{-3} determined for the no-PDT, RbF-PDT and KF-PDT cases, respectively. Thus, differences in charge carrier densities amount to orders of magnitude implying strong variations in the CdS layer resistivity. We relate these findings to compensating effects of Rb and K atoms in CdS, similarly to that of the Na atoms in CdS which cause acceptor type defects due to a single valence electron.[76] We explain these findings by the diffusion of the Rb and K atoms from the CIGSe surface into the CdS layer as well as by the presence of these alkali atoms in the chemical bath after having been etched off from films surface during a first stage of the CBD process. Note in addition that in previous works Rb and Na atoms were detected on the CdS surface.[30] Thus, Na, K and Rb atoms act in CdS as compensating acceptors, the K atoms having a stronger compensation impact which may also affect the optical properties detrimentally. This finding is supported by theIQE measurements which show the strongest CdS-absorption for KF-treated absorber for all CBD durations.[31] While the authors claim that this should be attributed to an alkali induced thickness effect of the deposited CBD CdS buffer, this additional compensation effect may also contribute to why the solar cells from KF-PDT absorbers show lower fill factors and short-circuit currents compared to their counterparts from RbF-PDT absorbers.[31]

4. CONCLUSIONS

We have combined the Kelvin probe and the photoelectron yield spectroscopy methods at ambient pressure to investigate the formation of the CdS/CIGSe interface with differently conditioned CIGSe surface by alkali-fluoride post-deposition treatments such as KF-PDT and RbF-PDT. The results were compared to reference samples without PDT. An overall good agreement to previously published data has been found. In addition, we observe distinct features related to an initial CBD-CdS growth stage associated with a CIGSe surface etching phase. We found in particular that the initial surface state of the PDT-treated CIGSe surface is not preserved after immersion in the CBD. After the initial CBD surface etching stage, the VBM of the CIGSe surface is significantly shifted towards the Fermi level, e.g. by about 180 meV, 290 meV and 620 meV for the no-PDT, RbF-PDT and KF-PDT treated CIGSe surfaces, respectively. However, the CIGSe surface VBM positions are still much below the VBM of the CIGSe bulk. We propose that the native oxides and secondary phases are removed, resulting in a CIGSe surface with a band gap of 1.46 eV – 1.58 eV characteristic for copper-poor CIGSe surface composition. At the CdS/CIGSe interface a lowest VBM discontinuity is found for the RbF-PDT sample. At this interface, during the CdS induction/coalescence phase, a thin layer with a thickness ~11–18 nm and a graded band gap is formed due to a gradual variation of the CdS composition. This layer is electronically characterized by a gradual VBM downward shift. During the ion-by-ion CBD growth stage the CdS thin films incorporate the alkali Na, K and Rb atoms which were found to act in CdS as compensating acceptors, leading to an increased thin film resistivity. The observed electronic characteristics correlate well with the behavior of the solar cells prepared from the same CIGSe absorbers.

ASSOCIATED CONTENT

Supporting Information.

CBD-CdS thin-film thickness as a function of deposition time, equivalent circuit diagram for the vibrating Kelvin probe arrangement, determination of the contact potential difference, CPD resolution, IMFPs for low energy electrons, electronic band structure of a semiconductor surface, enlarged PYS spectra of CdS/CIGSe stacks, PYS spectra of In_2Se_3 thin films, PYS spectra of CdS thin films, VBM and CBM positions of the CIGSe surface before and after the CBD-CdS etching stage (PDF)

AUTHOR INFORMATION

Corresponding Author

Marin Rusu – *Struktur und Dynamik von Energiematerialien, Helmholtz-Zentrum Berlin für Materialien und Energie, Lise-Meitner Campus, Hahn-Meitner-Platz 1, 14109 Berlin, Germany*; orcid.org/0000-0002-1429-0219; E-mail: rusu@helmholtz-berlin.de

Authors

Tim Kodalle – *PVcomB, Helmholtz-Zentrum Berlin für Materialien und Energie, Schwarzschildstr. 3, 12489 Berlin, Germany*

Leo Choubrac – *Struktur und Dynamik von Energiematerialien, Helmholtz-Zentrum Berlin für Materialien und Energie, Lise-Meitner Campus, Hahn-Meitner-Platz 1, 14109 Berlin, Germany*

Nicolas Barreau – *Université de Nantes, CNRS, Institut des Matériaux Jean Rouxel, IMN, F-44000 France*

Christian A. Kaufmann – *PVcomB, Helmholtz-Zentrum Berlin für Materialien und Energie, Schwarzschildstr. 3, 12489 Berlin, Germany*

Rutger Schlatmann – *PVcomB, Helmholtz-Zentrum Berlin für Materialien und Energie, Schwarzschildstr. 3, 12489 Berlin, Germany*

Thomas Unold – *Struktur und Dynamik von Energiematerialien, Helmholtz-Zentrum Berlin für Materialien und Energie, Lise-Meitner Campus, Hahn-Meitner-Platz 1, 14109 Berlin, Germany*

Notes

The authors declare no competing financial interest.

ACKNOWLEDGMENT

The authors gratefully acknowledge S. Levcenco for conduction of independent capacitance-voltage measurements on reference samples.

REFERENCES

(1) Nakamura, M.; Yamaguchi, K.; Kimoto, Y.; Yasaki, Y.; Kato, T.; Sugimoto, H. Cd-Free Cu(In,Ga)(Se,S)$_2$ Thin-Film Solar Cell with Record Efficiency of 23.35%. *IEEE J. Photovolt.* **2019**, *9(6)*, 1863-1867.

(2) Rudmann, D.; Brémaud, D.; da Cunha, A. F.; Bilger, G.; Strohm, A.; Kaelin, M.; Zogg, H.; Tiwari, A. N. Sodium Incorporation Strategies for CIGS Growth at Different Temperatures. *Thin Solid Films* **2005**, *480-481*, 55-60.

(3) Chirilă, A.; Reinhard, P.; Pianezzi, F.; Bloesch, P.; Uhl, A. R.; Fella, C.; Kranz, L.; Keller, D.; Gretener, C.; Hagendorfer, H.; Jaeger, D.; Erni, R.; Nishiwaki, S.; Buecheler, S.; Tiwari, A. N. Potassium-Induced Surface Modification of Cu(In,Ga)Se$_2$ Thin Films for High-Efficiency Solar Cells. *Nat. Mater.* **2013**, *12*, 1107–1111.

(4) Jackson, P.; Hariskos, D.; Wuerz, R.; Wischmann, W.; Powalla, M. Compositional Investigation of Potassium Doped Cu(In,Ga)Se$_2$ Solar Cells with Efficiencies up to 20.8%. *Phys. Status Solidi - Rapid Res. Lett.* **2014**, *8*, 219–222.

(5) Jackson, P.; Hariskos, D.; Wuerz, R.; Kiowski, O.; Bauer, A.; Magorian Friedlmeier, T.; Powalla, M. Properties of Cu(In,Ga)Se$_2$ Solar Cells with New Record Efficiencies up to 21.7%. *Phys. Status Solidi - Rapid Res. Lett.* **2015**, *9*, 28–31.

(6) Jackson, P.; Wuerz, R.; Hariskos, D.; Lotter, E.; Witte, W.; Powalla, M. Effects of Heavy Alkali Elements in Cu(In,Ga)Se$_2$ Solar Cells with Efficiencies up to 22.6%. *Phys. Status Solidi - Rapid Res. Lett.* **2016**, *10*, 583–586.

(7) Kato, T.; Wu, J.; Hirai, Y.; Sugimoto, H.; Bermudez, V. Record Efficiency for Thin-Film Polycrystalline Solar Cells up to 22.9% Achieved by Cs-Treated Cu(In,Ga)(Se,S)$_2$. *IEEE J. Photovolt.* **2019**, *9*, 325–330.

(8) Ruckh, M.; Schmid, D.; Kaiser, M.; Schäffler, R.; Walter, T.; Schock, H. W. Influence of Substrates on the Electrical Properties of Cu(In,Ga)Se$_2$ Thin Films. *Solar Energy Mater. Solar Cells* **1996**, *41-42*, 335-343.

(9) Reinhard, P.; Bissig, B.; Pianezzi, F.; Avancini, E.; Hagendorfer, H.; Keller, D.; Fuchs, P.; Döbeli, M.; Vigo, C.; Crivelli, P.; Nishiwaki, S.; Buecheler, S.; Tiwari, A. N. Features of KF and NaF Postdeposition Treatments of Cu(In,Ga)Se$_2$ Absorbers for High Efficiency Thin Film Solar Cells. *Chem. Mater.* **2015**, *27*, 5755−5764.

(10) Wuerz, R.; Hempel, W.; Jackson, P. Diffusion of Rb in Polycrystalline Cu(In,Ga)Se$_2$ Layers and Effect of Rb on Solar Cell Parameters of Cu(In,Ga)Se$_2$ Thin-Film Solar Cells. *J. Appl. Phys.* **2018**, *124*, 165305.

(11) Nicoara, N.; Manaligod, R.; Jackson, F.; Hariskos, D.; Witte, W.; Sozzi, G.; Menozzi, R.; Sadewasser, S. Direct Evidence for Grain Boundary Passivation in Cu(In,Ga)Se$_2$ Solar Cells Through Alkali-Fluoride Post-Deposition Treatments. *Nat. Commun.* **2019**, *10*, 3980.

(12) Nicoara, N.; Lepetit, Th.; Arzel, L.; Harel, S.; Barreau, N.; Sadewasser, S. Effect of the KF Post-Deposition Treatment on Grain Boundary Properties in Cu(In,Ga)Se$_2$ Thin Films. *Sci. Rep.* **2017**, *7*, 41361.

(13) Pianezzi, F.; Reinhard, P.; Chirilă, A.; Bissig, B.; Nishiwaki, S.; Buecheler, S.; Tiwari, A. N. Unveiling the Effects of Post-Deposition Treatment with Different Alkaline Elements on the Electronic Properties of CIGS Thin Film Solar Cells. *Phys. Chem. Chem. Phys.* **2014**, *16*, 8843–8851.

(14) Laemmle, A., Wuerz, R. & Powalla, M. Efficiency Enhancement of Cu(In,Ga) Se_2 Thin-Film Solar Cells by a Post-Deposition Treatment with Potassium Fluoride. *Phys. Status Solidi - Rapid Res. Lett.* **2013**, *7*, 631–634.

(15) Weinhardt, L.; Hauschild, D.; Heske, C. Surface and Interface Properties in Thin-Film Solar Cells: Using Soft X-Rays and Electrons to Unravel the Electronic and Chemical Structure. *Adv. Mater.* **2019**, 1806660.

(16) Schmid, D.; Ruckh, M.; Grunwald, F.; Schock, H. W. Chalcopyrite/Defect Chalcopyrite Heterojunctions on the Basis of $CuInSe_2$. *J. Appl. Phys.* **1993**, *73*, 2902-2909.

(17) Schmid, D.; Ruckh, M.; Schock, H. W. Photoemission Studies on Cu(In,Ga)Se_2 Thin Films and Related Binary Selenides. *Appl. Surf. Sci.* **1996**, *103*, 409-429.

(18) Morkel, M.; Weinhardt, L.; Lohmüller, B.; Heske, C.; Umbach, E.; Riedl, W.; Zweigart, S.; Karg, F. Flat Conduction-Band Alignment at the Thin-Film Solar-Cell Heterojunction. *Appl. Phys. Lett.* **2001**, *79*, 4482-4484.

(19) Heske, C.; Fink, R.; Umbach, E.; Riedl, W.; Karg, F. Na-Induced Effects on the Electronic Structure and Composition of Cu(In,Ga)Se_2 Thin-Film Surfaces. *Appl. Phys. Lett.* **1996**, *68*, 3431-3433.

(20) Rusu, M.; Wiesner, S.; Fuertes Marron, D.; Meeder, A.; Doka, S.; Bohne, W.; Lindner, S.; Schedel-Niedrig, Th., Giesen, Ch.; Heuken, M.; Lux-Steiner, M. Ch. $CuGaSe_2$ Thin Films Prepared by a Novel CCSVT Technique for Photovoltaic Application. *Thin Solid Films* **2004**, *451–452*, 556–561.

(21) Würz, R.; Rusu, M.; Schedel-Niedrig, Th.; Lux-Steiner, M. Ch.; Bluhm, H.; Hävecker, M.; Kleimenov, E.; Knop-Gericke, A.; Schlögl, R. In Situ X-Ray Photoelectron Spectroscopy Study of the Oxidation of $CuGaSe_2$. *Surf. Sci.* **2005**, *580*, 80–94.

(22) Rusu, M.; Bär, M.; Lehmann, S.; Sadewasser, S.; Weinhardt, L.; Kaufmann, C. A.; Strub, E.; Röhrich, E.; Bohne, W.; Lauermann, I.; Jung, Ch.; Heske, C.; Lux-Steiner, M. Ch. Three-Dimensional Structure of the Buffer/Absorber Interface in CdS/$CuGaSe_2$ Based Thin Film Solar Cells. *Appl. Phys. Lett.* **2009**, *95*, 173502.

(23) Hauschild, D.; Kreikemeyer-Lorenzo, D.; Jackson, P.; Magorian Friedlmeier, T.; Hariskos, D.; Reinert, F.; Powalla, M.; Heske, C.; Weinhardt, L. Impact of a RbF Postdeposition Treatment on the Electronic Structure of the CdS/Cu(In,Ga)Se_2 Heterojunction in High-Efficiency Thin-Film Solar Cells. ACS Energy Lett. **2017**, *2*, 2383−2387.

(24) Handick, E.; Reinhard, P.; Alsmeier, J-H.; Köhler, L.; Pianezzi, F.; Krause, S.; Gorgoi, M.; Ikenaga, E.; Koch, N.; Wilks, R. G.; Buecheler, S.; Tiwari, A. N.; Bär, M. Potassium Postdeposition Treatment-Induced Band Gap Widening at Cu(In,Ga)Se_2 Surfaces − Reason for Performance Leap? *ACS Appl. Mater. Interfaces* **2015**, *7*, 27414−27420.

(25) Handick, E.; Reinhard, P.; Wilks, R. G.; Pianezzi, F.; Kunze, T.; Kreikemeyer-Lorenzo, D.; Weinhardt, L.; Blum, M.; Yang, W:; Gorgoi, M.; Ikenaga, E.; Gerlach, D.; Ueda, S.; Yamashita, Y.; Chikyow, T.; Heske, C.; Buecheler, S.; Tiwari, A. N.; Bär, M.. Formation of a K-In-Se Surface Species by NaF/KF Postdeposition Treatment of Cu(In,Ga)Se_2 Thin-Film Solar Cell Absorbers. *ACS Appl. Mater. Interfaces* **2017**, *9*, 3581−3589.

(26) Lepetit, T.; Harel, S.; Arzel, L.; Ouvrard, G.; Barreau, N. KF Post Deposition Treatment in Co- Evaporated Cu(In,Ga)Se_2 Thin Film Solar Cells: Beneficial or Detrimental Effect Induced by the Absorber Characteristics. *Prog. Photovolt. Res. Appl.* 2017, *25*, 1068–1076.

(27) Pistor, P.; Greiner, D.; Kaufmann, C. A.; Brunken, S.; Gorgoi, M.; Steigert, A.; Calvet, W.; Lauermann, I.; Klenk, R.; Unold, T.; Lux-Steiner, M.-C. Experimental Indication for Band Gap Widening of Chalcopyrite Solar Cell Absorbers After Potassium Fluoride Treatment. *Appl. Phys. Lett.* **2014**, *105*, 063901.

(28) Maticiuc, N.; Kodalle, T.; Lauche, J.; Wenisch, R.; Bertram, T.; Kaufmann, C.A.; Lauermann, I. In Vacuo XPS Investigation of Cu(In,Ga)Se_2 Surface After RbF Post-Deposition Treatment. *Thin Solid Films* **2018**, *665*, 143-147.

(29) Kodalle, T.; Heinemann, M. D.; Greiner, D.; Yetkin, H. A.; Klupsch, M.; Li, C.; van Aken, P. A.; Lauermann, I.; Schlatmann, R.; Kaufmann, C. A. Elucidating the Mechanism of an RbF post Deposition Treatment in CIGS Thin Film Solar Cells. *Sol. RRL* **2018**, *2*, 1800156.

(30) Kreikemeyer-Lorenzo, D.; Hauschild, D.; Jackson, P.; Friedlmeier, T. M.; Hariskos, D.; Blum, M.; Yang, W.; Reinert, F.; Powalla, M.; Heske, C.; Weinhardt, L. Rubidium Fluoride Post-Deposition Treatment: Impact on the Chemical Structure of the Cu(In,Ga)Se_2 Surface and CdS/Cu(In,Ga)Se_2 Interface in Thin-Film Solar Cells. *ACS Appl. Mater. Interfaces* **2018**, *10*, 37602−37608.

(31) Kodalle, T.; Choubrac, L.; Arzel, L.; Schlatmann, R.; Barreau, N.; Kaufmann, C. A. Effects of KF and RbF Post Deposition Treatments on the Growth of the CdS Buffer Layer on CIGS Thin Films – a Comparative Study. *Sol. Energy Mater. Sol. Cells* **2019**, *200*, 109997.

(32) Weinhardt, L.; Heske, C.; Umbach, E.; Niesen, T. P.; Visbeck, S.; Karg, F. Band Alignment at the i-ZnO/CdS Interface in Cu(In,Ga)$(S,Se)_2$ Thin-Film Solar Cells. *Appl. Phys. Lett.* **2004**, *84*, 3175-3177.

(33) Rusu, M.; Rumberg, A.; Schuler, S.; Nishiwaki, S.; Würz,R.; Babu, S. M.; Dziedzina, M.; Kelch, C.; Siebentritt, S.; Klenk, R.; Schedel-Niedrig, Th.; Lux-Steiner, M.Ch. Optimisation of the CBD CdS Deposition Parameters for ZnO/CdS/$CuGaSe_2$/Mo Solar Cells. *J. Phys. Chem. Solids* **2003**, *64*, 1849–1853.

(34) Mahanty, S.; Basak, D.; Rueda, F.; Leon, M. Optical Properties of Chemical Bath Deposited CdS Thin Films. *J. Electron. Mater.* **1999**, *28(5)*, 559-562.

(35) Zelaya-Angel, O.; Alvarado-Gil, J. J.; Lozada-Morales, R.; Vargas, H.; Ferreira da Silva, A. Band-Gap Shift in CdS Semiconductor by Photoacoustic Spectroscopy: Evidence of a Cubic to Hexagonal Lattice Transition. *Appl. Phys. Lett.* **1994**, *64(3)*, 291-293.

(36) Repins, I.; Contreras, M.A.; Egaas, B.; DeHart, C.; Scharf, J.; Perkins, C.L.; To, B.; Noufi, R. 19.9%-Efficient ZnO/CdS/CuInGaSe$_2$ Solar Cell with 81.2% Fill Factor. *Prog. Photovolt. Res. Appl.* **2008**, *16*, 235–239.

(37) Barreau, N.; Painchaud, T.; Couzinie-Devy, F.; Arzel, L.; Kessler, J. Recrystallization of CIGSe Layers Grown by Three-Step Processes: A Model Based on Grain Boundary Migration, *Acta Mater.* **2010**, *58*, 5572–5577.

(38) Lord Kelvin. Contact Electricity of Metals. *Philos. Mag.* **1898**, *46*, 82-119.

(39) Baumgärtner, H.; Liess, H. D. Micro Kelvin Probe for Local Work-Function Measurements. *Rev. Sci. Instrum.* **1988**, *59(5)*, 802-805.

(40) Gobeli, G. W.; Allen, F. G. Direct and Indirect Excitation Processes in Photoelectric Emission from Silicon. *Phys. Rev.* **1962**, *127*, 141-149.

(41) Sebenne, C. A. High-Resolution Photoemission Yield and Surface States in Semiconductors. *Il Nuovo Cimento* **1977**, *39B*, 768-780.

(42) Sebastiani, M.; Di Gaspare, L.; Capellini, G.; Bittencourt, C.; Evangelisti, F. Low-Energy Yield Spectroscopy as a Novel Technique for Determining Band Offsets: Application to the c-Si(100)/a-Si:H Heterostructure. *Phys. Rev. Lett.* **1995**, *75(18)*, 3352-3355.

(43) Baikie, I. D.; Grain, A. C.; Sutherland, J.; Law, J. Dual Mode Kelvin Probe: Featuring Ambient Pressure Photoemission Spectroscopy and Contact Potential Difference. *Energy Procedia* **2014**, *60*, 48-56.

(44) Baikie, I. D.; Grain, A. C.; Sutherland, J.; Law, J. Ambient Pressure Photoemission Spectroscopy of Metal Surfaces. *Appl. Surf. Sci.* **2014**, *323*, 45-53.

(45) Zisman, W. A.; A New Method of Measuring Contact Potential Differences in Metals. *Rev. Sci. Instrum.* **1932**, *3*, 367-370.

(46) Anderson, J. R.; Alexander, A. E. Study of Adsorption on Metals by the Contact Potential Technique. *Aust. J. Chem.* **1953**, *6(2)*, 109-122.

(47) Macdonald, J. R.; Edmondson, D. E. Exact Solution of a Time-Varying Capacitance Problem. *Proc. Inst. Radio Eng.* **1961**, *49*, 453-466.

(48) Baikie, I. D.; Mackenzie, S.; Estrup, P. J. Z.; Meyer, J. A. Noise and the Kelvin Method. *Rev. Sci. Instrum.* **1991**, *62 (5)*, 1326-1332.

(49) Baikie, I. D.; Estrup, P. J. Low Cost PC Based Scanning Kelvin Probe. *Rev. Sci. Instrum.* **1998**, *69 (11)* 3902-3907.

(50) Kronik, L.; Shapira, Y. Surface Photovoltage Phenomena: Theory, Experiment, and Applications. *Surf. Sci. Rep.* **1999**, *37*, 1-206.

(51) Kirihata, H.; Uda, M. Externally Quenched Air Counter for Low-Energy Electron Emission Measurements. *Rev. Sci. Instrum.* **1981**, 52(1), 68-70.

(52) Miyamoto, E.; Yamaguchi, Y.; Yokoyama, M. Ionization Potential of Organic Pigment Film by Atmospheric Photoelectron Emission Analysis. *Electrophotography* **1989**, *28*, 364-370.

(53) Grigalevicius, S.; Blazys, G.; Ostrauskaite, J.; Grazulevicius, J.V.; Gaidelis, V.; Jankauskas, V.; Montrimas, E. 3,6-Di(N-Diphenylamino)-9-Phenylcarbozole and its Methyl-Substituted Derivative as Novel Hole-Transporting Amorphous Molecular Materials. *Synth. Mater.* **2002**, *128*, 127-131.

(54) Honda, M.; Kanai, K.; Komatsu, K.; Ouchi, Y.; Ishii, H.; Seki, K. Atmospheric Effect of Air, N_2, O_2, and Water Vapor on the Ionization Energy of Titanyl Phthalocyanine Thin Film Studied by Photoemission Yield Spectroscopy. *J. Appl. Phys.* **2007**, *102*, 103704.

(55) Nakayama, Y.; Machida, S.; Minari, T.; Tsukagishi, K.; Noguchi, H.; Ishii, H. Direct Observation of the Electronic States of Single Crystalline Rubrene under Ambient Condition by Photoelectron Yield Spectroscopy. *Appl. Phys. Lett.* **2008**, *93*, 173305.

(56) Harwell, J.R.; Baikie, T. K.; Baikie, I. D.; Payne, J. L.; Ni, C.; Irvine, J. T. S.; Turnbull, G. A.; Samuel, I. D. W. Probing the Energy Levels of Perovskite Solar Cells via Kelvin Probe and UV Ambient Pressure Photoemission Spectroscopy. *Phys. Chem. Chem. Phys.* **2016**, *18*, 19738-19745.

(57) Berglund, C. N.; Spicer, W. E. Photoemission Studies of Copper and Silver: Theory. *Phys. Rev.* **1964**, *136(4a)*, 1030-1044.

(58) Fowler, R. H. The Analysis of Photoelectric Sensitivity Curves for Clean Metals at Various Temperatures. *Phys. Rev.* **1931**, *38*, 45-56.

(59) Ballantyne, J. M. Effect of Phonon Energy Loss on Photoemissive Yield Near Threshold. *Phys. Rev. B* **1972**, *6 (4)*, 1436-1455.

(60) Kane, E. O. Theory of Photoelectric Emission from Semiconductors. *Phys. Rev.* **1962**, *127(1)*, 131-141.

(61) Gobeli, G. W.; Allen, F. G. Direct and Indirect Excitation Processes in Photoelectric Emission from Silicon. *Phys. Rev.* **1962**, *127(1)*, 141-149.

(62) Ishii, H.; Kudo, K.; Nakayama, T.; Ueno, N. (eds.) Electronic Processes in Organic Electronics. *Springer Series in Materials Science*, vol. 209 (Springer, Japan, 2015).

(63) Nicoara, N.; Kunze, T.; Jackson, P.; Hariskos, D.; Duarte, R. F.; Wilks, R. G.; Witte, W.; Bär, M.; Sadewasser, S. Evidence for Chemical and Electronic Nonuniformities in the Formation of the Interface of RbF-Treated Cu(In,Ga)Se_2 with CdS. *ACS Appl. Mater. Interfaces* **2017**, *9*, 44173-44180.

(64) Rusu, M.; Glatzel, Th.; Neisser, A.; Kaufmann, C. A.; Sadewasser, S.; Lux-Steiner, M. Ch. Formation of the Physical Vapor Deposited CdS/Cu(In,Ga)Se_2 Interface in Highly Efficient Thin Film Solar Cells. *Appl. Phys. Lett.* **2006**, *88*, 143510.

(65) Sasaki, K. Study of Work Function of the {0001} Faces of CdS Crystal. I. *Japan. J. Appl. Phys*. **1974**, *13(6)*, 933-938.

(66) Lincot, D.; Borges, R. O. Chemical Bath Deposition of Cadmium Sulfide Thin Films. In Situ Growth and Structural Studies by Combined Quartz Crystal Microbalance and Electrochemical Impedance Techniques. *J. Electrochem. Soc.* **1992**, *139(7)*, 1880-1889.

(67) Choubrac, L.; Brammertz, G.; Barreau, N.; Arzel, L.; Harel, S.; Meuris, M.; Vermang, B. 7.6% CZGSe Solar Cells Thanks to Optimized CdS Chemical Bath Deposition. *Phys. Status Solidi A* **2018**, *215*, 1800043.

(68) Kodalle, T.; Raghupathy, R. K. M.; Bertram, T.; Maticiuc, N.; Yetkin, H. A.; Gunder, R.; Schlatmann, R.; Kühne, T. D.; Kaufmann, C. A.; Mirhosseini, H. Properties of Co-Evaporated $RbInSe_2$ Thin Films. *Phys. Status Solidi RRL* **2018**, 1800564.

(69) Nakada, T.; Kunioka, A. Direct Evidence of Cd Diffusion Into Cu(In,Ga)Se_2 Thin Films During Chemical-Bath Deposition Process of CdS Films. *Appl. Phys. Lett.* **1999**, *74*, 2444-2446.

(70) Sozzi, G.; Troni, F.; Roberto Menozzi, R. On the Combined Effects of Window/Buffer and Buffer/Absorber Conduction-Band Offsets, Buffer Thickness and Doping on Thin-Film Solar Cell Performance. *Sol. Energy Mater. Sol. Cells* **2014**, *121*, 126-136.

(71) Schmid, D.; Ruckh, M.; Schock, H. W. A Comprehensive Characterization of the Interfaces in Mo/CIS/CdS/ZnO Solar Cell Structures. *Sol. Energy Mater. Sol. Cells* **1996**, *41/42*, 281-294.

(72) Park, S. M.; Kim, T. G.; Chung, Y. D.; Cho, D.-H.; Kim, J.; Kim, K. J.; Yi, Y.; Kim, J. W. Junction Formation at the Interface of CdS/$CuIn_xGa_{(1-x)}Se_2$. J. Phys. *D: Appl. Phys.* **2014**, *47*, 345302.

(73) Sze, S. M.; Ng, K. K. Physics of Semiconductor Devices. 3rd Edition. Published by John Wiley & Sons, Inc., Hoboken, New Jersey, 2007.

(74) Persson, C. Anisotropic Hole-Mass Tensor of $CuIn_{1-x}Ga_x(S,Se)_2$: Presence of Free Carriers Narrows the Energy Gap. *Appl. Phys. Lett.* **2008**, *93*, 072106.

(75) Ekuma, E. C.; Franklin, L.; Zhao, G. L.; Wang, J. T.; Bagayoko, D. An-Initio Local Density Approximation Description of the Electronic Properties of Zinc Blende Cadmium Sulfide (zb-CdS). *Physica B* **2011**, *406*, 1477-1480.

(76) Varley, J. B.; Lordi, V.; He, X.; Rockett, A. First Principles Calculations of Point Defect Diffusion in CdS Buffer Layers: Implications for $Cu(In,Ga)(Se,S)_2$ and $Cu_2(Zn,Sn)(Se, S)_4$-Based Thin-Film Photovoltaics. *J. Appl. Phys.* **2016**, *119*, 025703.

For Table of Contents Only